J Mater Sci (2009) 44:1726–1733
DOI 10.1007/s10853-008-3108-x

Spallation of two thermal barrier coating systems: experimental study of adhesion and energetic approach to lifetime during cyclic oxidation

P.-Y. Théry · M. Poulain · M. Dupeux · M. Braccini

Received: 30 May 2008 / Accepted: 7 November 2008 / Published online: 11 December 2008

Abstract To understand the degradation of two thermal barrier coating (TBC) systems, we determined the adhesion energy between the bondcoat and the topcoat and its evolution during cyclic oxidation at 1,100 °C, by means of a modified 4-point bending test. An yttria stabilized zirconia (YSZ) ceramic topcoat was deposited by electron beam physical vapour deposition (EBPVD) on a Ni-based superalloy with either an intermediate β-(Ni,Pt)Al bondcoat or a newly developed Zr-doped β-NiAl bondcoat. Although a similar evolution of the adhesion energy during cyclic oxidation has been recorded for both systems, observations of the fracture surfaces combined with a microstructure study revealed different degradation mechanisms. An energetic model of spallation is applied to predict their lifetime. According to this approach, the TBC failure is induced by the accumulation of strain energy in the ceramic layers and resisted by the interfacial fracture toughness. The predicted lifetime is consistent with experiments for both systems.

Introduction

Thermal barrier coatings systems (TBC systems) are deposited by electron beam physical vapour deposition (EBPVD) onto aeronautical turbines blades in order to protect them from combustion gases. Failure of these multilayered systems occurs when the ceramic insulating topcoat spalls off, thus exposing the metallic parts directly to the hot gases. The key point for preserving the integrity of the bond between the insulating coating and the superalloy constituting the blade in service conditions resides in the good bonding strength conferred by the interfacial thermally grown oxide (TGO). This TGO consists of a protective alumina scale, which forms through selective oxidation of the bondcoat layer—embedded between the ceramic topcoat and the underlying superalloy. Indeed a submicronic TGO layer initially forms during the EBPVD processing that enhances the adherence of the topcoat. However, the TGO growth during service results in loss of topcoat adherence.

The lifetime of TBC systems is usually determined by means of cyclic oxidation tests, performed under laboratory air at atmospheric pressure. Periodic visual inspections indicate the moment when spallation happens, generally at the end of a cooling step, i.e. at room temperature. In this way, lifetimes of various TBC systems can be compared, but this type of test gives no information about the evolution of the interfacial toughness during thermal cycling. The sudden failure is due to rapid propagation of interfacial cracks, initiated by complex phenomena linked to the oxidation mechanisms and to the evolution of the interfacial area stress field and intrinsic interface adhesion properties. In particular, oxide growth, thermal expansion mismatch and phase transformations during thermal cycling contribute to a high-compressive stress level within the TGO.

With a view to understand better how the interfacial strength is affected by microstructure evolutions, we have designed and implemented a specific test (a modified 4-point bending test) that gives a quantitative assessment of

P.-Y. Théry · M. Poulain (✉)
ONERA-DMSM, 29 avenue de la Division Leclerc BP 72, Chatillon 92322, France
e-mail: martine.poulain@onera.fr

M. Dupeux · M. Braccini
SIMAP, 1130 rue de la Piscine BP 75, St Martin d'Heres 38402, France

the EBPVD TBC systems adhesion, thus allowing to record its evolution during cyclic oxidation.

This article presents results obtained on two EBPVD TBC systems, one with a β-(Ni,Pt)Al bondcoat and the other with a newly developed Zr-doped β-NiAl bondcoat. Observations of the fracture surfaces of the adhesion test specimens as well as a microstructural study conducted on oxidised samples revealed what kind of microstructure degradations may initiate the spallation.

Finally, the whole set of experimental data, including in particular adhesion energy and residual stresses measurements, enables us to develop an energetic approach of the TBC systems failure. This approach is based on the evaluation of the available energy that can cause the interfacial crack propagation (accumulation of strain energy density in the interfacial TGO and in the partially stabilized yttria-doped zirconia (YSZ) topcoat during thermal cycling) and on the comparison between that stored energy and the energy needed to fracture the interface (with decreasing interfacial toughness as the microstructure degradations proceed). From this mechanical modelling a spallation criterion can be defined that gives an estimate of the TBC systems lifetime.

After exposing the experimental procedure, we describe successively the evolution of the adhesion in both systems, the energetic model for the spallation criteria and finally discuss the results.

Experimental procedure

Selected adhesion test

With the view of quantifying the adhesion energy evolution of TBC systems during thermal cycling, we had first to select a test that could be employed on TBC systems having a thin (150 μm), porous and brittle EBPVD ceramic layer.

A number of tests have been proposed to characterize the practical adhesion of multilayered systems.

The interfacial toughness of various systems can be compared through qualitative information provided by indirect methods. For example, indentation tests [1, 2] have been applied on TBC systems so as to estimate an interfacial toughness derived from delamination lengths measurements.

Direct methods such as the tensile pull off test can be used, provided that the measurements are not limited by the bonding strength between the specimen and the loading components [3]. Compressive tests on specifically designed test specimens have also been successfully applied on TBC systems [4]. Machining and preparation costs may be a practical limitation.

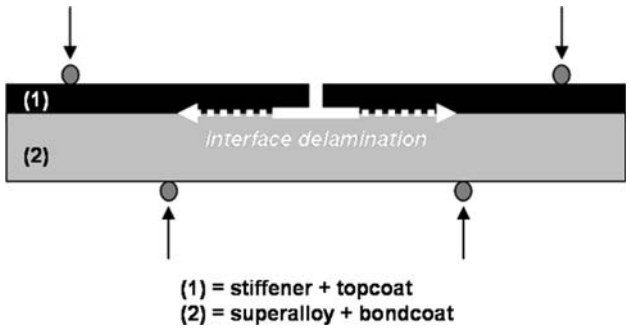

Fig. 1 A bimaterial 4-point bending specimen [7]

More specific adhesion tests have been proposed, for example, the pushout test [5], or other innovative interfacial fracture tests [6]. It has to be reckoned that the adaptation of these tests to TBC systems with a thin EB-PVD ceramic layer may be very difficult. In addition, a complete analysis of the test adapted to peculiar shape specimens is generally required to extract the energy release rate.

Given that background, we selected a simple test relatively easy to implement, but which needed to be adapted for EBPVD TBCs. This is a 4-point bending test (Fig. 1), an adhesion test originally introduced by Charalambides et al. [7] and which is now extensively used in the field of microelectronics thin films [8] and other applications [9]. However, it has been rarely applied to TBC adhesion measurement so far [10–12], and even less in the case of EBPVD topcoats [13]. The challenge in this case consists in generating spallation of the topcoat without breaking the EBPVD ceramic layer or the brittle underlying intermetallic bondcoat. Once this is resolved, strain energy release rate values can be derived from the applied load during the stable crack propagation stage between the two inner loading points [7]. The crucial point is then to record a plateau-force on the load-deflection curve. Consequently a specific operating procedure has been defined and implemented. First, a stiffener must be bonded onto the EBPVD columnar topcoat in order to increase the amount of elastic energy stored in the specimen. This lowers the required load for propagating the interfacial crack, thus preventing the brittle topcoat and bondcoat from fragmenting, and the superalloy substrate from yielding. As a consequence, the analysis of the experiment is simplified. Second, a perpendicular notch must be machined through the stiffener down to the interface to be delaminated. Finally, preliminary experiments proved that, in our case, an interfacial pre-crack must absolutely be introduced at the centre of the specimen to promote the symmetry of the interfacial debonding and to avoid catastrophic crack propagation. Otherwise, overloading is needed to initiate the interfacial crack and no plateau-force can be recorded, and therefore no reliable information on the adhesion energy can be

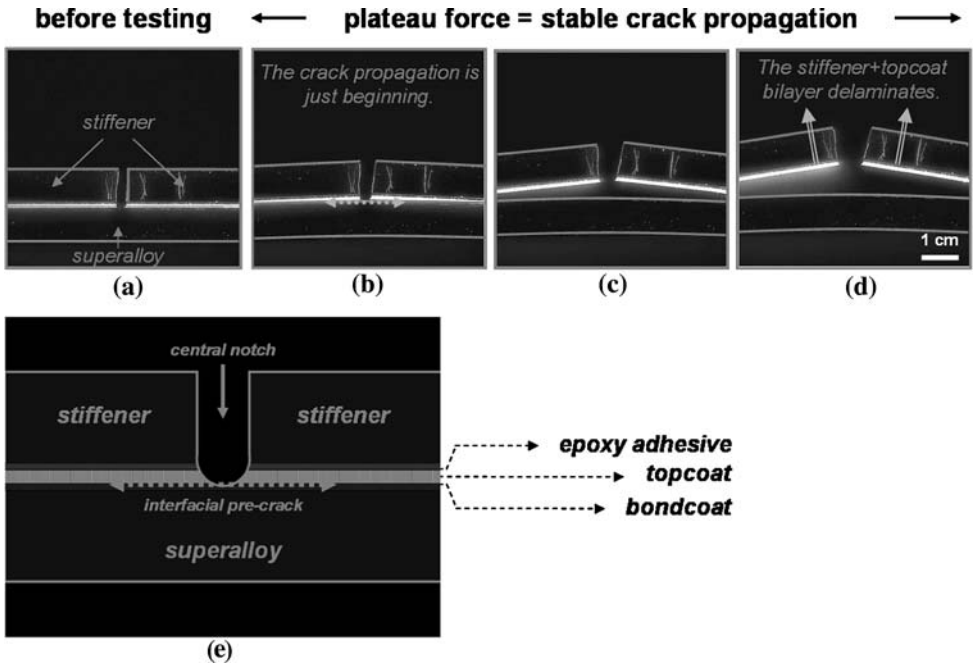

Fig. 2 Sequence of video images recorded focusing on the specimen central part during the bending test (the white layer is the YSZ topcoat). **a** initial specimen as described by the schematic drawing; **e**, **b** crack initiation; **c**, **d** crack opening

extracted. Our solution to this difficulty consists in a specific surface treatment on a central band of the specimens prior to the EBPVD deposition.

As illustrated by the sequence of video macroscopic images recorded throughout the adhesion test in Fig. 2, this procedure actually leads to the topcoat delamination, as desired. When a plateau-force is recorded, the stable interfacial crack propagation occurs between the two inner loading points, so that the (stiffener +topcoat) bilayer eventually spalls off. It is to note that in such 4-point bend tests, the far-range mode mixity on the delamination crack [7] is such that the crack is mechanically driven towards the centre of curvature of the specimen (opposite to the ceramic topcoat in our specimens), until it becomes stabilized along the weakest interface in the multilayer. So, the specimen arrangement prevents the crack from deviating towards the ceramic topcoat. SEM observations on fracture surfaces provide information on the exact crack path below the ceramic topcoat layer, according to the system studied and the number of applied thermal cycles (see next paragraph). Eventually analytical [7] as well as numerical finite element calculations have been performed so as to derive the strain energy release rate from the experimental results obtained on as-deposited and thermally cycled specimens. A thermal cycle consists in heating the specimens up to 1,100 °C in 10 min, holding them at 1,100 °C during 1 h and cooling them down to 200 °C in 5 min.

TBC system specimens elaboration and preparation

Plate-shaped single-crystal AM1 superalloy substrates protected with a β-(Ni,Pt)Al bondcoat or a β-NiAl(Zr) bondcoat have been topcoated with an EBPVD YSZ ceramic layer (7 wt% Y_2O_3-ZrO_2–135 μm thick). The specimens (60 × 8 × 1 mm) were machined so that all the faces were oriented along the $< 001 >$ directions. The as-thermochemically deposited bondcoats contain about 39 at.% aluminium. The whole bondcoat surface was sand blasted prior to the EBPVD topcoat deposition, except within a central transverse stripe (1 mm wide), which has been intentionally exempted of this standard industrial process by means of an adhesive masking tape. Due to particular oxidation phenomena, that imply transient alumina formation (Fig. 3), numerous voids appear within this stripe beneath the TGO scale, which includes the stable α alumina phase—in contact with the bondcoat—and a mixed oxide zone (zirconia–alumina) in contact with the topcoat. This complex structure of the TGO locally reduces the YSZ topcoat adhesion below the central notch (Fig. 4). In that manner, an efficient interfacial pre-crack source was introduced into the adhesion test specimens.

Before the adhesion experiments, a steel plate (AISI 304 L—1 mm thick) was bonded to the YSZ topcoat using an epoxy adhesive (Araldite 2011). Then the central notch was machined with a wire saw (ϕ 100 μm) through the steel stiffener and the YSZ topcoat.

Adhesion evolution

Adhesion energy evolution

The results obtained by means of the adhesion tests on initial and oxidised samples are synthesised in Table 1.

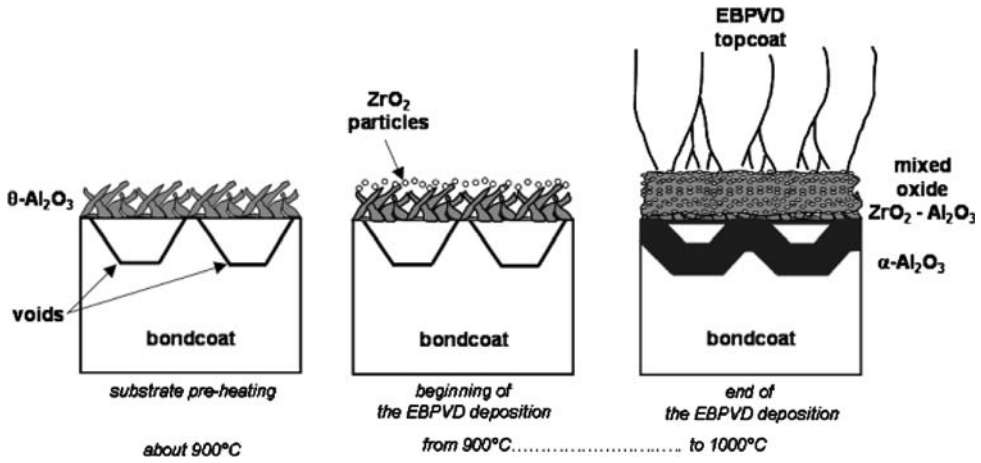

Fig. 3 Oxidation of the central stripe—exempted of the standard sand blasting process—during the EBPVD topcoat deposition

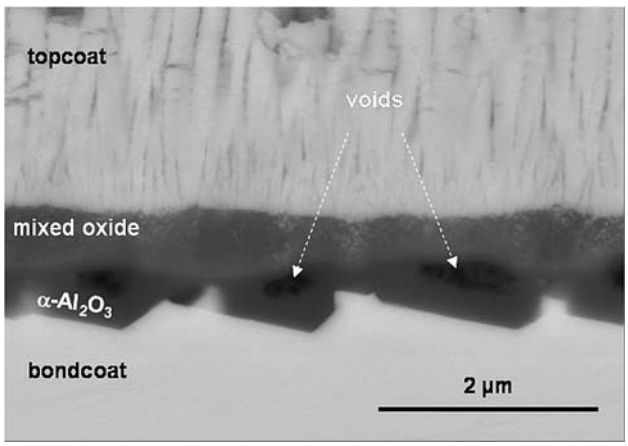

Fig. 4 Faceted voids developed beneath the alumina scale within the central stripe—exempted of the standard sand blasting process

Table 1 Adhesion energies G_c (J/m^2) of two TBC systems as a function of the number of 1 h-cycles at 1,100 °C (3–5 specimens tested for each result; typical scatter dispersion about 10%)

TBC system	Initial	50 cycles	100 cycles	150 cycles	200 cycles
AM1/β-(Ni,Pt)Al/YSZ	112	55	26	23	–
AM1/β-NiAl(Zr)/YSZ	114	43	31	–	27

First of all, it must be noticed that, for a given state of oxidation, the values of experimental adhesion energies (G_c) are very close for both systems, the typical scatter dispersion being less than 10%. The adhesion energy of as-deposited systems is about 110 J/m^2 for both bondcoats, β-(Ni,Pt)Al and β-NiAl(Zr), and a similar decrease is observed while thermal cycling advances. The adhesion energy drops down to around 50 J/m^2 after the first fifty 1 h-cycles at 1,100 °C, and after 100 cycles, its level remains approximately constant till the end of the cyclic oxidation test, i.e. until the TBC spontaneously delaminates.

Table 2 Evolution of the TGO thickness (µm ± 0.2 µm) in two TBC systems as a function of the number of 1 h-cycles at 1,100 °C (measurements on cross sectional micrographs over a 3 mm length)

TBC system	Initial	50 cycles	100 cycles	200 cycles
AM1/β-(Ni,Pt)Al/YSZ	0.2	2.6	3.3	4.5
AM1/β-NiAl(Zr)/YSZ	<0.2	1.8	2.4	3.1

Microstructure degradation

The cyclic oxidation induces thickening of the TGO that is moderate in the case of the NiAl(Zr) bondcoat compared to the (Ni,Pt)Al one. This difference (see Table 2) is attributed to the beneficial effect of Zr on nickel aluminide oxidation [14].

SEM observations on both sides of the fracture surfaces of the adhesion test specimens reveal that the crack propagates along the entire TGO/bondcoat interface, when considering the β-NiAl(Zr) bondcoat, as attested by the alumina imprints which cover all the bondcoat surface (Fig. 5). Both the topcoat and the TGO layer are carried away when the spallation occurs. On the contrary, in the case of the β-(Ni,Pt)Al bondcoat, some blocks of alumina remain on the fracture surface (Fig. 6). This indicates that the crack deviates across the TGO layer at some points so that the fracture path stands essentially along the TGO/bondcoat interface and from time to time along the topcoat/TGO interface.

The other difference between the two systems is the presence of interfacial voids observed only on the β-(Ni,Pt)Al fracture surface, associated with an extensive rumpling of this bondcoat, as attested by roughness measurements (see Table 3) on cross sectional micrographs [15].

Geometrical incompatibilities in concave areas and voids formation due to oxidation mechanisms are responsible for failure at the ceramic/β-(Ni,Pt)Al interface (Fig. 7). In contrast, no voids are detected at the

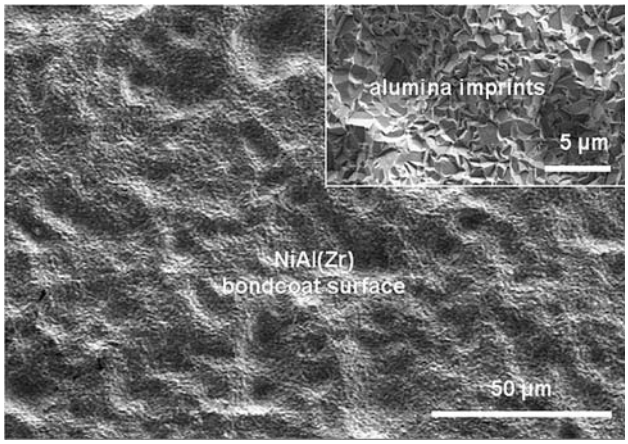

Fig. 5 Fracture surface of the AM1/NiAl(Zr)/YSZ specimen after hundred 1 h-cycles at 1,100 °C (secondary electron SEM micrograph)

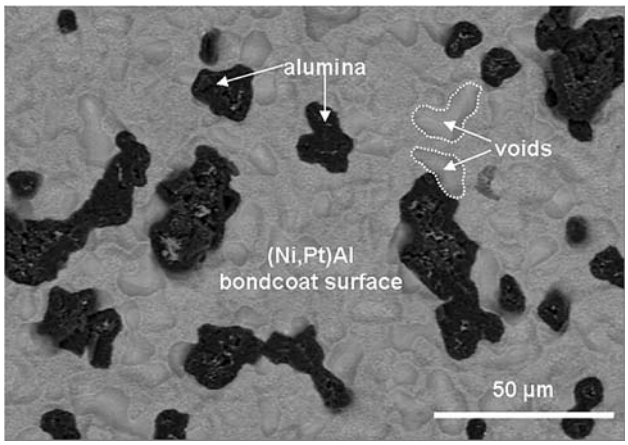

Fig. 6 Fracture surface of the AM1/(Ni,Pt)Al/YSZ specimen after hundred 1 h-cycles at 1,100 °C (backscattered electron SEM micrograph)

Table 3 Evolution of the arithmetical mean roughness R_a (μm ± 0.2 μm) of the TGO/bond coat interface of two TBC systems as a function of the number of 1 h-cycles at 1,100 °C (measurements on cross sectional micrographs over a 3 mm length)

TBC system	Initial	50 cycles	100 cycles	200 cycles
AM1/β-(Ni,Pt)Al/YSZ	0.8	1.2	1.9	3.0
AM1/β-NiAl(Zr)/YSZ	0.9	1.0	1.1	1.6

TGO/β-NiAl(Zr) bondcoat interface, which remains rather smooth during its whole lifetime (see Table 3).

This difference may originate from the difference in mechanical behaviour of the two systems, which influences the bondcoat deformation. In the case of the β-(Ni,Pt)Al bondcoat, the growth strains of the TGO at high temperature causes the bondcoat surface deformation, as attested by the interfacial roughness significantly increase. The

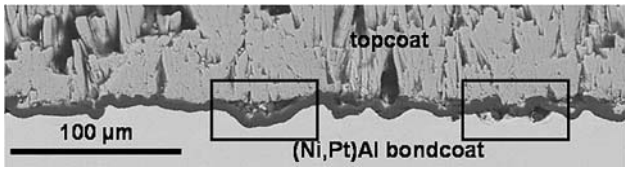

Fig. 7 Interfacial damage in AM1/(Ni,Pt)Al/YSZ specimen after fifty 1 h-cycles at 1,100 °C

in-plane compressive stresses translate into out-of-plane tensile stresses at peaks and valleys of the TGO/bondcoat and TGO/topcoat interfaces, respectively. When the tensile stress exceeds a critical value, a void can form at the interface (Fig. 7). This degrades the adhesion energy.

On the contrary, in the case of the β-NiAl(Zr), zirconium is known to enhance the yield stress of NiAl compounds and also to increase the creep strength of alumina [16, 17], the deformation of the interfacial zone is then less pronounced (Fig. 8).

The difference in residual stresses between the two cases is illustrated in Table 4. According to these results, residual in-plane compressive stresses within the TGO—as determined by photoluminescence piezospectroscopy (PLPS) measurements—are about 1 GPa higher in the case of the β-NiAl(Zr) bondcoat, compared to the β-(Ni,Pt)Al one. This difference could originate from the difference in

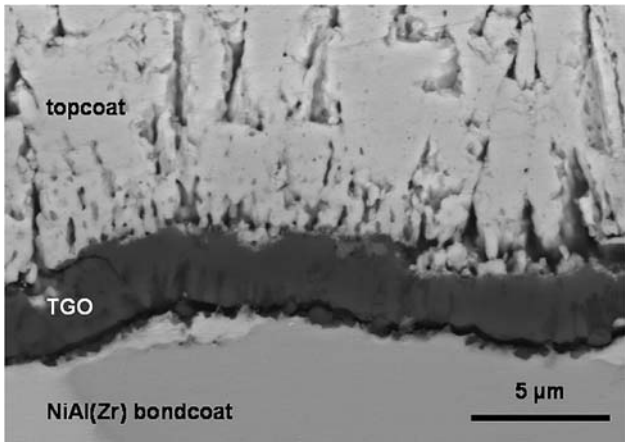

Fig. 8 Interfacial damage in AM1/NiAl(Zr)/YSZ specimen after fifty 1 h-cycles at 1,100 °C

Table 4 Evolution of the residual compressive stress σ (GPa ± 0.1 GPa) within the TGO layer in two TBC systems as a function of the number of 1 h-cycles at 1,100 °C

TBC system	50 cycles	100 cycles	150 cycles	200 cycles
AM1/β-(Ni,Pt)Al/YSZ	2.8	2.8	2.8	2.5
AM1/β-NiAl(Zr)/YSZ	3.7	3.9	3.8	3.8

mechanical properties of the bondcoats: thermal expansion coefficient and viscoplastic behaviour at high temperature.

Energetic spontaneous spallation model

With the aim to propose a possible guide for predicting TBC systems lifetime, which is a goal of prime importance, an energetic model is investigated on the two TBC systems of interest. For the lifetime assessment, an energy balance is used, by comparing evolution of the available energy for propagating the pre-crack in the 4-point bending test with the evolution of the critical energy release rate.

Energetic balance equations

According to this approach [18–22], the important parameter for spontaneous delamination is the elastic energy progressively stored into the coating which finally spalls off, i.e. in the circumstances within the (YSZ + TGO) bilayer.[1]

Following the calculation process conducted in [22], the energy stored into the ceramic bilayer is expressed by:

$$W_{\text{stored}} = W_{\text{stored}}(\text{YSZ}) + W_{\text{stored}}(\text{TGO}) \tag{1}$$

For each component (i = YSZ or TGO):

$$W_{\text{stored}}(i) = \frac{\left(1 - v_i^2\right)}{2E_i}\sigma_i^2 e_i \tag{2}$$

where e is the thickness of the layer, E and v are, respectively, its in-plane Young's modulus and its Poisson's ratio. The stress σ is also assumed to be biaxial and isotropic in the plane of the layer.

The basic idea is that the TBC failure is induced by the accumulation of strain energy density within the ceramic bilayer and resisted by the interfacial toughness, but the final curvature of the scale must also be taken into account, so that the available energy to drive the crack propagation is reduced to:

$$W_{\text{available}} = W_{\text{stored}} - W_{\text{curved scale}} \tag{3}$$

$$\text{where } W_{\text{curved scale}} = W_{\text{curved}}(\text{YSZ}) + W_{\text{curved}}(\text{TGO}) \tag{4}$$

For each component (i = YSZ or TGO):

$$W_{\text{curved}}(i) = \frac{1}{E_i}\left(\frac{P_i^2}{e_i} + \frac{12M_i^2}{e_i^3}\right) \tag{5}$$

where P_i is the force and M_i the moment related to the component i.

These parameters are expressed by:

$$\begin{aligned} P_i &= \frac{E_i e_i^2}{12}K \\ M_i &= \frac{E_i e_i^3}{12}K \end{aligned} \tag{6}$$

K is the curvature acquired by the ceramic bilayer when it spalls off:

$$K = 3\frac{\varepsilon(\text{TGO}) - \varepsilon(\text{YSZ})}{2e_{\text{YSZ}}\left(1 + \frac{E_{\text{YSZ}}e_{\text{YSZ}}}{4E_{\text{TGO}}e_{\text{TGO}}}\right)} \tag{7}$$

where ε is the strain in the considered layer, when in-plane stressed.

For each component (i = YSZ or TGO):

$$\varepsilon(i) = \frac{1 - v_i}{E_i}\sigma_i \tag{8}$$

Eventually, the available energy to drive the failure can be calculated from Eq. 3 by combining all the above equations, provided the elastic properties of the ceramic layers and the in-plane stresses are known. The stress σ_{TGO} has been experimentally determined (by means of PLPS experiments) and σ_{YSZ} has been derived from thermal expansion differences as follows:

$$\sigma_{\text{YSZ}} \approx A\frac{E_{\text{YSZ}}}{1 - v_{\text{YSZ}}}\left(\alpha_{\text{YSZ}} - \alpha_{\text{superalloy}}\right)\Delta T \tag{9}$$

where α_{I} (i = YSZ or superalloy) is the thermal expansion coefficient (respectively 11.10^{-6} K^{-1} and 16.10^{-6} K^{-1}) and A a non-dimensional parameter which takes into account the stress gradient within the zirconia layer (A $\approx$ 0.5 according to [22]).

Now, to deduce a lifetime prediction, this available energy release rate must be compared at each stage of the evolution of the TBC to the critical crack propagation energy needed for spontaneous spallation G_{cs}, according to the failure criterion

$$W_{\text{available}} \geq G_{cs} \tag{10}$$

G_{cs} can be deduced from the 4-point bending adhesion measurements as described in the previous paragraph, taking into account the loading mode difference between these laboratory tests and spontaneous spalling. The interfacial crack propagation energy is indeed sensitive to the so-called mode mixity angle ψ [23], which is the parameter measuring the ratio between mode II ($\psi = 90°$) and mode I ($\psi = 0°$) loadings during the crack propagation.

It can be inferred from Charalambides et al. [7] that under our experimental conditions (similar elastic properties and thicknesses of both dominant elastic layers of the sandwich specimen), the loading mode during 4-point bending delamination stands approximately about $\psi = 40°$. On the other hand, Faulhaber et al. [24] show that during the

[1] In the case of remaining alumina blocks onto the β-(Ni,Pt)Al bondcoat, this energy was lowered according to the fraction part area of standing adhesive TGO, as measured on fracture surfaces.

spontaneous buckling and growth of TBC scales, the interfacial loading rapidly tends to pure mode II. Then pure mode II values of G_{cs} can be estimated from our 4-point adhesion values of G_c using the empirical relation proposed by [25]:

$$G_c = G_{Ic}\{1 + \tan^2[(1-\lambda)\psi]\} \quad (11)$$

where G_{Ic} is the adhesion energy in pure mode I crack opening, λ is a non-dimensional parameter, comprised between 0.3 and 0.33 for TBC systems depending on the interfacial roughness [26, 27]. According to this analysis, even if G_{cI} is unknown, the corrective ratio between $G_{cs} = G_{IIc} = G_c$ ($\psi = 90°$) and measured G_c ($\psi = 40°$) can be calculated as:

$$\frac{G_{cs}}{G_c(\psi = 40°)} = \frac{1 + \tan^2[(1-\lambda)90]}{1 + \tan^2[(1-\lambda)40]} \quad (12)$$

It is to note that this analysis provides a necessary condition but not a sufficient one: when Eq. 10 is satisfied, the failure may occur.

Failure criterion evaluation

By using the whole set of experimental data and the materials parameters listed in Table 5 the concomitant evolutions of $W_{\text{available}}$ and $G_{cs} = G_{IIc}$ during oxidation cycles can be compared (Fig. 9). It is to note that a parametrical study clearly indicates that the parts of the elastic energy progressively stored into the topcoat and the scale curvature have a marked influence on the energy balance, so that these contributions must not be considered as negligible.

Whereas the uncertainty on the adhesion energy is linked to the misevaluation of the λ fit parameter (Eq. 11), the uncertainty on the available energy is due to the lack of reliable data concerning the YSZ Young's modulus increase. When exposed at high temperature, sintering phenomena occur in the topcoat and as a consequence, its in-plane Young's modulus is likely to increase. This evolution is difficult to assess and literature data on similar systems have been used, assuming that the maximal value is reached in a parabolic way after one hundred 1 h-cycles at 1,100 °C.

It is to note that in both cases (β-(Ni,Pt)Al and β-NiAl(Zr) bondcoats), the experimental lifetime duration (around 200 ± 20 cycles for the β-(Ni,Pt)Al bondcoat, and about 250 ± 20 cycles for the β-NiAl(Zr) one), which has been determined by means of cyclic oxidation tests performed on 3–5 specimens until the TBC spontaneous spallation is observed, lies within the area where the adhesion energy and the available energy intersect, (shaded area in Fig. 9). Consequently, we can conclude that a coherent prediction of the interfacial failure is formulated by means of the present energetic approach.

Table 5 Young's modulus and Poisson ratio of the two ceramic layers

Material	E [GPa]	ν
YSZ	20–50 or 20–80 [18, 19, 22]	0.2 [20, 22]
TGO	400 [18, 20, 28]	0.2 [20, 22]

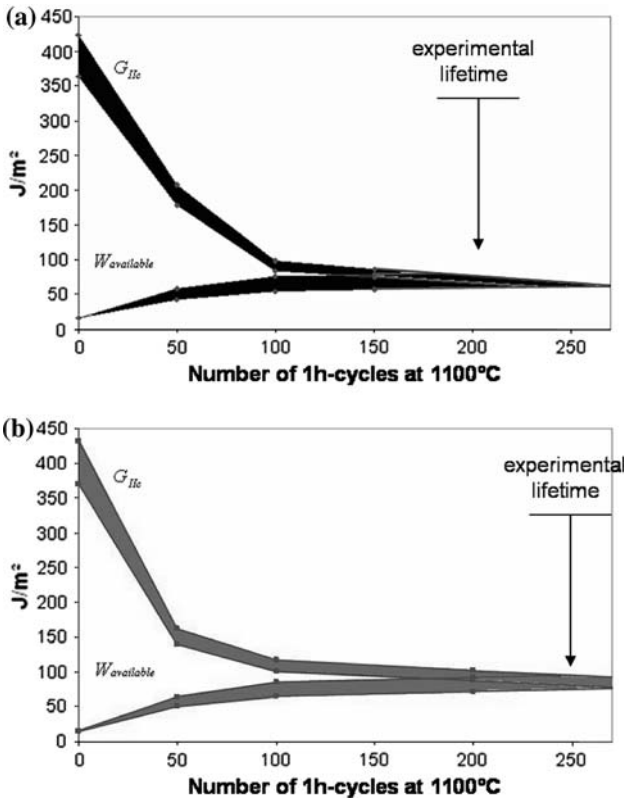

Fig. 9 Evolution of G_{IIc} and $W_{available}$ during cyclic oxidation at 1,100 °C. **a** AM1/(Ni,Pt)Al/YSZ system **b** AM1/NiAl(Zr)/YSZ system

Discussion

The consistency and reliability of our analysis are ensured owing to the fact that the competing energies derive from experimental data obtained on the same TBC specimens. However, to go further and refine the prediction capabilities of this approach, a better knowledge of the mechanical properties (and their evolution) of the various layers is necessary. In particular a reliable determination of the YSZ Young's modulus deviation related to sintering effects is needed.

According to this model, lifetime duration could be improved by maintaining high values of interfacial fracture toughness and/or by restricting the stored energy within the ceramic layers. The decrease in fracture toughness observed as the number of cycles increases, is likely to be linked to damage mechanisms in the interfacial zone:

cavities forming and extending in the case of the (Ni,Pt)Al bondcoat and weakening of the TGO/bondcoat interface in the case of the NiAl(Zr) bondcoat. The causes behind these mechanisms (phase transformations, composition and structure evolution in the bondcoat, segregation at interfaces) are still to be investigated.

Another way to prolong lifetimes of these TBC systems would be to decrease the stored energy. Residual stresses may be lowered if relaxation mechanisms are operative in the bondcoat and in the TGO at high temperature. However, as a consequence of such relaxation, the interfacial region may deform, with possible nucleation and growth of cavities, thus weakening the adhesion energy. Another way would be to decrease the oxidation kinetics, thus minimizing the TGO thickness contribution in Eq. 2. Despite numerous studies on the oxidation of alumina-forming alloys, no clear progress has been obtained in this domain. Finally, it should be emphasized that sintering phenomena should be avoided in the zirconia layer, as they contribute to increase the in-plane Young's modulus of this layer, thus increasing the stored energy.

Conclusion

A 4-point bending adhesion test has been adapted to propagate an interfacial crack in EBPVD TBC systems in a reproducible and reliable mode, enabling to derive interfacial fracture energies. This test has been applied to two systems, one with a classical (Ni,Pt)Al bondcoat and the other with a newly developed NiAl(Zr) bondcoat to check the influence of thermal cycling on their adhesion. In both cases, the fracture energy decreases rapidly during cyclic oxidation and stabilizes after one hundred 1-h cycles at 1,100 °C. Although the trends are similar, the microstructure examinations and the residual stress measurements revealed different mechanisms: progressive growth of interfacial cavities together with extensive rumpling of the TGO/bondcoat interface in the first case, weakening of TGO/bondcoat which remains smooth in the second case.

An energy-based spallation model has been applied, which consists in comparing the decreasing TBC adhesion energy and the increasing elastic stored energy (due to the growth of thermal oxide and possible sintering phenomena). The lifetime predictions given by this model are consistent with the experimental lifetimes observed in both cases. It is to note that the evaluation of the available energy to drive the failure and of the interfacial fracture toughness from experimental results have been obtained on the same TBC specimens, thus ensuring the consistency and reliability of the analysis.

As a practical consequence, the newly developed Zr-doped β-NiAl bondcoat appears to be a realistic possible alternative to the classical β-(Ni,Pt)Al bondcoat system for TBC on Ni-base superalloy turbine blades.

Acknowledgements The authors are indebted to Dr. R. Mevrel (ONERA) for helpful discussions during the course of this study, and to Dr. N. Terrien (ONERA) for his assistance in the PLPS measurements.

References

1. Mumm DR, Evans AG (2000) Acta Mater 48:1815
2. Vasinonta A, Beuth JL (2001) Eng Fract Mech 68:843
3. Watanabe M, Kuroda S, Yokoyama K et al (2008) Surf Coat Technol 202:1746
4. Guerre C (2002) PhD Thesis, Ecole Nationale Supérieure des Mines de Paris
5. Kim S, Liu Y, Kagawa Y (2007) Acta Mater 55:3771
6. Arai M, Okajima Y, Kishimoto K (2007) Eng Fract Mech 74:2055
7. Charalambides PG, Jund J, Evans AG, McMeeking RM (1989) J Appl Mech 56:77
8. Gan Z, Mhaisalkar SG, Chen Z et al (2005) Surf Coat Technol 198:85
9. Li H, Khor KA, Cheang P (2007) Eng Fract Mech 74:1894
10. Hofinger I, Oechsner M, Bahr HA et al (1998) Int J Fracture 92:213
11. Quian L, Zhu S, Kagawa Y (2003) In: 27th international conference on advanced ceramics and composites: a (Cocoa Beach, FL, USA), vol 24, issue 3, p 503
12. Yamasaki Y, Schmidt A, Scholz A (2006) Surf Coat Technol 201:744
13. Bahr HA, Balke H, Fett T et al (2003) Mater Sci Eng A 362:2
14. Théry PY (2007) Thèse de Doctorat, Universite Joseph Fourier Grenoble, France, Matériaux et Génie des Procédés
15. Théry PY, Poulain M, Dupeux M, Braccini M (2007) Surf Coat Technol 202:648
16. Noebe RD, Bowman RR, Nathal MV (1993) Int Mater Rev 38:193
17. Li YZ, Wang C, Chan HM et al (1999) J Am Ceram Soc 82:1497
18. Evans AG, Mumm DR, Hutchinson JW et al (2001) Prog Mater Sci 46:505
19. Hutchinson JW, Evans AG (2002) Surf Coat Technol 149:179
20. Xu T, Faulhaber S, Mercer C et al (2004) Acta Mater 52:1439
21. Spitsberg IT, Mumm DR, Evans AG (2005) Mater Sci Eng A 394:176
22. Zhao X, Wang X, Xiao P (2006) Surf Coat Technol 200:5946
23. Shih CF (1991) Mater Sci Eng A 143:77
24. Faulhaber S, Mercer C, Moon MW et al (2006) J Mech Phys Solids 54:1004
25. Hutchinson JW, Suo Z (1992) Adv Appl Mech 29:63
26. Wang JS, Evans AG (1998) Acta Mater 46:4993
27. Wang JS, Evans AG (1999) Acta Mater 47:699
28. Lipkin DM, Clarke DR, Hollatz M et al (1997) Corr Sci 39:231